Detecting temporal correlations in hopping dynamics in Lennard–Jones liquids

OPEN ACCESS
IOP Publishing
Journal of Physics A: Mathematical and Theoretical
J. Phys. A: Math. Theor. **55** (2022) 324003 (15pp)
https://doi.org/10.1088/1751-8121/ac7e0a

Detecting temporal correlations in hopping dynamics in Lennard–Jones liquids

Vittoria Sposini[1,*], Aleksei V Chechkin[2,3,4], Igor M Sokolov[5] and Sándalo Roldán-Vargas[6]

[1] Faculty of Physics, University of Vienna, Kolingasse 14-16, 1090 Vienna, Austria
[2] Institute for Physics & Astronomy, University of Potsdam, 14476 Potsdam-Golm, Germany
[3] Faculty of Pure and Applied Mathematics, Hugo Steinhaus Center, Wrocław University of Science and Technology, Wyspianskiego 27, 50-370 Wrocław, Poland
[4] Akhiezer Institute for Theoretical Physics, 61108 Kharkov, Ukraine
[5] Institute of Physics & IRIS Adlershof, Humboldt University Berlin, 12489 Berlin, Germany
[6] Department of Applied Physics, Faculty of Sciences, University of Granada, 18071 Granada, Spain

E-mail: vittoria.sposini@univie.ac.at

Received 18 March 2022, revised 24 June 2022
Accepted for publication 4 July 2022
Published 21 July 2022

Abstract

Lennard–Jones mixtures represent one of the popular systems for the study of glass-forming liquids. Spatio/temporal heterogeneity and rare (activated) events are at the heart of the slow dynamics typical of these systems. Such slow dynamics is characterised by the development of a plateau in the mean-squared displacement (MSD) at intermediate times, accompanied by a non-Gaussianity in the displacement distribution identified by exponential tails. As pointed out by some recent works, the non-Gaussianity persists at times beyond the MSD plateau, leading to a Brownian yet non-Gaussian regime and thus highlighting once again the relevance of rare events in such systems. Single-particle motion of glass-forming liquids is usually interpreted as an alternation of rattling within the local cage and cage-escape motion and therefore can be described as a sequence of waiting times and jumps. In this work, by using a simple yet robust algorithm, we extract jumps and waiting times from single-particle trajectories obtained via molecular dynamics simulations. We investigate the presence of correlations between waiting times and find negative correlations, which becomes more and more pronounced when lowering the temperature.

*Author to whom any correspondence should be addressed.

Keywords: glassy systems, hopping dynamics, jump detection, rare events

S Supplementary material for this article is available online

(Some figures may appear in colour only in the online journal)

1. Introduction

In the last decade a vivid interest has been paid on studying and understanding systems characterised by exponentially-tailed displacement distributions and linear (Fickian) trend of the mean-squared displacement (MSD). Indeed, a Fickian MSD would lead to the assumption of standard Brownian motion with its characteristic Gaussian distribution. However this is often not the case. Experimental systems displaying this Brownian (or Fickian) yet non-Gaussian (BnG) diffusion include nanospheres in entangled actin hydrogels [1], colloidal beads moving along lipid nanotubes [1, 2], binary mixtures of colloidal hard spheres [3], passive tracers in suspensions of eukaryotic swimmers [4] and many more [5–12]. The observation of exponential tails indicates the relevance of rare events in the system and has often been associated to the presence of spatial and/or temporal heterogeneity. A common approach to model BnG processes developed during the last years is based on the concept of stochastic diffusivity. The latter can be thought of as a random variable [13], as a switching process between two values [14] or as a stationary stochastic process fluctuating around an average value [15–20]. Apart from random diffusivity models—that are based on a Langevin description—other models have also been explored within different frameworks [21–28]. A different approach is discussed in [29–32] in which inhomogeneities in space are explicitly considered.

Recent experiments and extensive numerical simulations have pointed out that a BnG regime is clearly displayed by glass-forming systems [33–35], as well as by small tracers diffusing in glassy colloidal matrices [3, 36]. Moreover, a similar behaviour has also been observed in experimental studies of suspension of colloidal beads under the action of a static and spatially random optical force [37, 38], a system that display a single-particle motion qualitatively similar to the intermittent single-particle dynamics of glassy system.

The presence of exponential tails in the displacement distribution in glass-forming systems systems has been known for long [39, 40], yet this was mainly associated with intermediate times at which the MSD develops a plateau. Instead, it has been shown how the non-Gaussianity persists at times beyond the MSD plateau, clearly leading to a BnG regime and thus highlighting once again the relevance of rare events in such systems.

Given that the emergence of dynamic heterogeneities in glass–forming liquids upon cooling is a well established phenomenon [41, 42], the connection between BnG diffusion, exponential-tailed distributions and glass-forming liquids helps in strengthening the standard interpretation of BnG diffusion as due to heterogeneity in the system. In addition, such connection opens new directions of study since the overall picture of this phenomenology is still far from being completely understood.

The single-particle dynamics of glass-forming systems shows a motion that can be interpreted as consisting of two alternating phases: (i) confined motion within the cage defined by the neighbouring particles; (ii) hopping from one cage to another. This motion can be modelled as a continuous time random walk (CTRW) with waiting times, defined by the time each particle spends jiggling around within a cage, and jumps that are identified each time the particle

escapes the local cage. Indeed, this model has been used over the years to analyse data from glass-forming systems [40, 43–46].

In particular, jumps are usually extracted from simulation data (and/or from experimental data in the case of colloidal suspensions), and a lot of attention is posed on the study of the distribution of waiting times between subsequent jumps, its functional behaviour and its dependence on the temperature of the system [44–50]. Note that the works by Pastore *et al* [44–46] include results on the jump length distribution in addition to the ones on the waiting time distribution. In the study reported in [48–50] the authors focused on the identification of hopping events between local minima of the potential energy landscape. On the other hand, other studies focus explicitly on the analysis of single-particle displacement to identify caging events and jumps between them [44–47]. In this work we follow a similar approach and provide a prescription based on physical arguments on how to develop a jump detection algorithm based on the study of single-particle displacements. Moreover, we aim at making a step forward within this line of research by focusing on the study of temporal correlations. Indeed, to the best of our knowledge, there are only few works discussing possible temporal correlations in the single-particle dynamics of glass-forming systems [51–53]. On the one hand, Heuer *et al* [51] and Helfferich *et al* [52] focus their discussions on the analysis of the back and forth dynamics. On the other hand, Pastore *et al* [53] briefly address the issue of waiting time correlations as part of a more general study on the many features of the intermittent dynamics in colloidal and molecular glasses.

The jump detection algorithm described in this work provides a perfect framework for the study of such correlations, focusing in particular on the temporal correlations among waiting times (in a similar fashion to [53]). We study how such correlations depend on the parameter of the jump detection procedure and on the temperature of the system. The study reported here is based on results from Lennard–Jones (LJ) mixtures, as they represent one of the reference models for glass-forming systems. In particular, we focus on the 3D system as the 2D one is known to be more affected by finite size effects [54–56]. The paper is organised as follows. In section 2 we describe the simulations methods. In section 3 we present the jump detection procedure while in section 4 we discuss the statistical properties of the jump length and waiting time distributions. The main results of our analysis of the temporal correlation of waiting times are reported in section 5 and finally, in section 6, we draw our conclusions.

2. Methods

We perform molecular dynamics (MD) simulations of a three dimensional Kob–Andersen binary mixture [39, 57, 58]. The isotropic interaction between a particle of species α and a particle of species β is given by the LJ potential

$$V_{\alpha\beta}(r) = 4\epsilon_{\alpha\beta}\left[\left(\frac{\sigma_{\alpha\beta}}{r}\right)^{12} - \left(\frac{\sigma_{\alpha\beta}}{r}\right)^{6}\right], \quad \alpha,\beta \in \{\mathrm{A},\mathrm{B}\}, \tag{1}$$

where A and B are the labels for the two species and r is the distance between the centers of mass of the two particles. Both species have the same mass m which is set to unity. For computational efficiency the potential is truncated at a distance of $2.5\sigma_{\alpha\beta}$ [39]. The radius ($\sigma_{\alpha\beta}$) and strength ($\epsilon_{\alpha\beta}$) of interaction between particles A–A, A–B and B–B are different. σ_{AA} and ϵ_{AA} are set to 1 such that length is given in units of σ_{AA}, energy in units of ϵ_{AA} and time in units of $(m\sigma_{\mathrm{AA}}/48\epsilon_{\mathrm{AA}})^{1/2}$, where the $\sqrt{48}$ was originally added for convenience to adapt the unit of time for this system to describe the dynamics of a particular real

glassy alloy first investigated by Stillinger and Weber [39, 59]. Hereafter, all the values are reported in these reduced units. The system is composed of $N_A = 6400$ particles of type A and $N_B = 1600$ particles of type B distributed within a cube of edge length $L = 18.80$, such that the total number density is given by $\rho = (N_A + N_B)/L^3 = 1.20$. The chosen size of the simulated 3D Kob–Andersen system is based on previous studies on the size dependence of the time associated to the α—relaxation for this system [60]. For the density and the temperature range investigated in our paper, this time reaches a constant value when the system reaches a number of particles of the order of 2000 [60]. This composition avoids the emergence of a crystal structure even at very low temperature. We first run simulations in the canonical ensemble to equilibrate the system at a fixed temperature, T, controlled by an Andersen thermostat [61] with an effective mass of 48 reduced units with Boltzmann's constant set to 1. After the equilibration we run simulations in the microcanonical ensemble to evaluate the dynamic observables of interest. The temperature range $T \in [0.45, 0.7]$ corresponds to the supercooled regime of the system. Indeed, the lowest temperature corresponds to $1.03 \cdot T_c$, being T_c the mode coupling temperature of the glass transition [58] and the highest temperature is just below the onset temperature T_o [62]. We use a velocity Verlet algorithm [63] with a time step $\Delta t = 0.02$ for a total number of steps $N = 5 \times 10^6$. All the results reported here correspond to particles of the species A and are obtained by averaging over ten independent runs, such that the ensemble size of the analysed single-trajectories effectively increases from N_A to $10 \cdot N_A = 64\,000$.

3. Jump and waiting time detection

For our study it is essential to define what we mean by *jump* and *waiting time*. These definitions should have a clear physical meaning and the defined quantities should be easily measurable.

By looking at the typical MSD behaviour depicted in figure 1 [see supplementary material (https://stacks.iop.org/JPA/55/324003/mmedia) (SM) for MSD curves from simulation data] one can see that starting from an initial time, the particles show at short times a ballistic motion within a typical time t_b and a typical displacement d_b. This motion usually corresponds to an intra-cage vibrational motion within a short time regime where the MSD $\sim t^2$. Some particles, however, will find a way to escape from their respective local environments performing displacements of the order of a particle diameter σ (see the particle displacement trajectory in figure 1). The fastest way for a particle to perform this displacement is by keeping a ballistic motion beyond the typical length d_b defining the local cages. This is the time t^* shown in figure 1. Then, we will say that a particle has performed a jump when it displaces a length d^* of the order σ (at least $\sigma/2$, which is larger than d_b) within a time of the order of t^*. This estimate of t^* based on ballistic motion allows us to reduce as much as possible the number of jumps missed by the algorithm. Indeed, if the jump is actually performed in a random-walk fashion (as it most likely is), the time needed to cover the same distance would be longer than the corresponding ballistic one and thus, the jump will not be missed within our analysis. Thus, we use the assumption of ballistic motion to obtain the reference time- and length-scales for the identification of a jump.

According to the previous idea, we will follow all the particles individually and track their positions with a discretisation step $\Delta t = t^*$. In particular, we start by setting the reference position as the initial one and we compare it with the position at every time step Δt. Each time we detect a jump (i.e. a displacement larger than d^*) we (i) update the reference position (ii) store the jump time identified by t^i and (iii) store the jump length given by the displacement δr^i performed. The index i counts the number of jumps along the trajectory. We will then call waiting time t_w^i the time difference between consecutive jumps, i.e. $t_w^i = t^{i+1} - t^i$ (see figure 1).

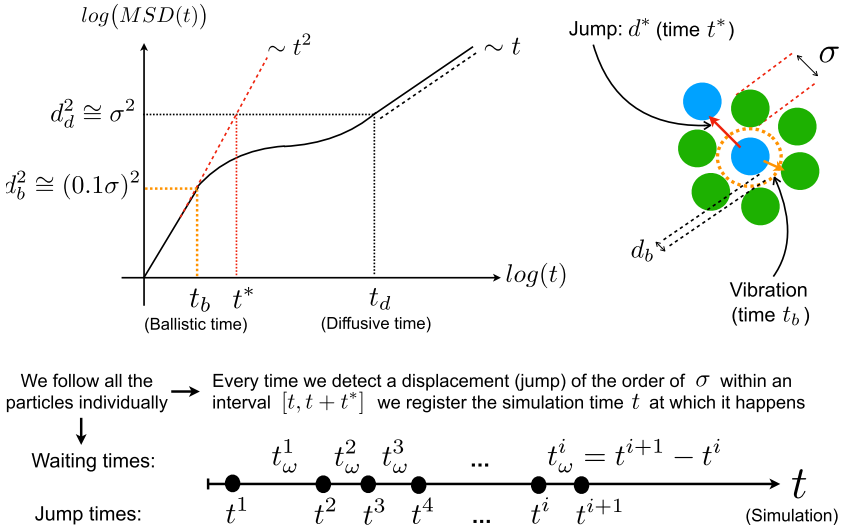

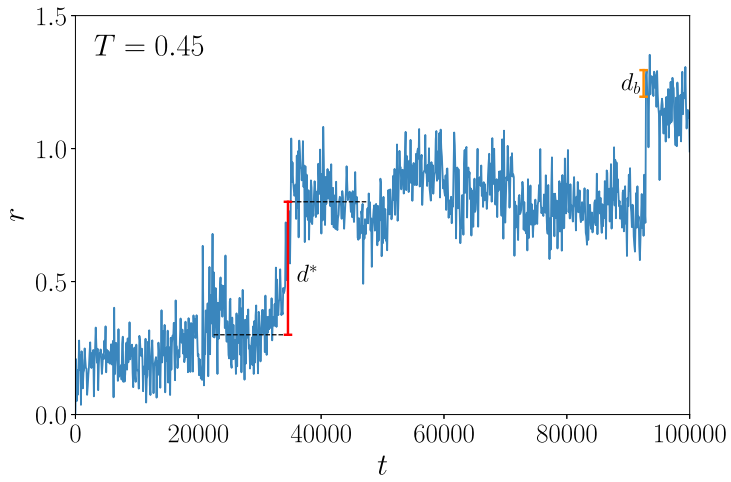

Figure 1. Schematic representation of the notions of *jump* and *waiting time* and example of single-particle displacement trajectory from MD simulations, defined as $r = \sqrt{(x-x_0)^2 + (y-y_0)^2 + (z-z_0)^2}$.

In this respect, we will have a timeline for each particle, as the one shown in figure 1, where the jump times (denoted by dots) are scattered within the complete simulation time. To implement this procedure we can make an educated guess for t^* based on the equipartition of the kinetic energy, which for a 3D system takes the form:

$$\frac{1}{2}m\langle v^2\rangle = \frac{3}{2}k_{\mathrm{B}}T \Rightarrow \overline{v} = \sqrt{\langle v^2\rangle} = \sqrt{\frac{3}{m}k_{\mathrm{B}}T} \Rightarrow t^* = \frac{\sigma}{\overline{v}} = \sigma\sqrt{\frac{m}{3k_{\mathrm{B}}T}}, \tag{2}$$

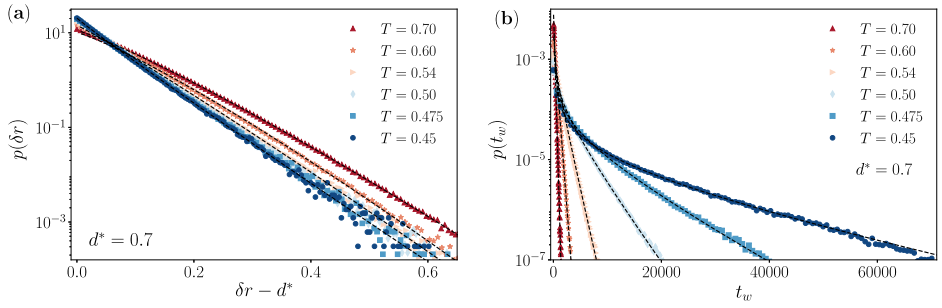

Figure 2. Comparison of (a) jump length and (b) waiting time distributions at fixed $d^* = 0.7$ and for different values of temperature.

where $\overline{v}$ is the average particle ballistic velocity, m the mass of the particles, k_B Boltzmann constant, and T the absolute temperature. In particular, for the Kob–Andersen system we obtain $t^* = \sqrt{48/3T}$ since $m = k_B = \sigma = 1$. For our simulations we set $t^* = 5$ which is comparable with our educated guess for the temperature range of interest. Concerning the jump length parameter d^*, following our argument above and recalling that $d_d \cong \sigma = 1$, we set $1/2 \leqslant d^* < 1$. In particular, we report results for three different values, i.e. $d^* = 0.5, 0.6, 0.7$, that are large enough to observe jumps and yet not too large that the statistics become too poor to perform a robust analysis.

As mentioned already in section 1, a similar approach for the detection of jumps was used in [44–47]. In particular, in [44–46] the authors analyse the fluctuations in time of the position within an interval of the order of $20t_b$ and compare it with the so-called Debye–Waller factor (see [44] for details on their algorithm). The procedure described in [47] is based directly on the study of the particle displacement, as the one we use in this work, however in their study the values of the parameters that we defined as t^* and d^* are chosen based on empirical analysis of simulation data. The description introduced in this work provides, by means of simple physical arguments, an explanation on how to choose the values for t^* and d^*.

4. Jump length and waiting time distribution

In figures 2–4 and table 1 we report results on the distributions of jump lengths and waiting times extracted from MD simulations, as discussed in section 3. In a standard diffusive dynamics we would expect the former to be well described by a Rayleigh distribution (characterised by a Gaussian tail) and the latter by an exponential distribution. The results obtained from our analysis of the Kob–Andersen mixture in the supercooled regime deviate from such trends, as already observed in other works performing similar analysis [44–47].

In figure 2 we display the temperature dependence of the jump length and waiting time distributions. Note that here we focus on $d^* = 0.7$ but our results are verified for all the three values of d^*—see SM. First of all we observe that the functional behaviour of the jump length distribution can be well described by a compressed exponential (or stretched Gaussian) $p(\delta r) \propto \exp\left(-(\delta r/\delta r_0)^\alpha\right)$ with $\alpha \geqslant 1$, while the one of the waiting time distribution by an exponentially truncated power law $p(t_w) \propto t_w^{-\beta} \exp\left(-t_w/t_0\right)$, with $\beta \geqslant 0$ and $t_0 > 0$ (as an alternative one could also use a stretched exponential function—see SM for more details). The values of the coefficients α, β and t_0 obtained from fitting our data are reported in table 1 together with the first moment of both distributions. For the jump length distribution the value

Table 1. In the table we report the values of the coefficients α, β and t_0 of the jump length and waiting times distribution obtained from fits at different T and d^* values and corresponding average jump length and waiting time values. The error bars for α and β are of the order of 10^{-2} or smaller while for t_0 they are unity on the last digit.

		$T = 0.45$	$T = 0.475$	$T = 0.50$	$T = 0.54$	$T = 0.60$	$T = 0.70$
$d^* = 0.5$	α	1.0	1.0	1.0	1.1	1.1	1.2
	$\langle \delta r \rangle$	0.55	0.55	0.55	0.56	0.56	0.57
	β	1.5	1.4	1.1	1.0	0.6	0.1
	t_0	2×10^4	7×10^3	3×10^3	6×10^2	2×10^2	6×10^1
	$\langle t_w \rangle$	1×10^3	7×10^2	5×10^2	3×10^2	1×10^2	7×10^1
$d^* = 0.6$	α	1.0	1.0	1.0	1.1	1.1	1.2
	$\langle \delta r \rangle$	0.65	0.65	0.65	0.66	0.66	0.67
	β	1.1	1.0	0.8	0.8	0.1	0.2
	t_0	2×10^4	7×10^3	3×10^3	8×10^2	2×10^2	1×10^2
	$\langle t_w \rangle$	3×10^3	2×10^3	1×10^3	5×10^2	2×10^2	1×10^2
$d^* = 0.7$	α	1.0	1.0	1.0	1.1	1.2	1.2
	$\langle \delta r \rangle$	0.75	0.75	0.75	0.67	0.76	0.77
	β	0.9	0.7	0.6	0.3	0.1	0.1
	t_0	2×10^4	8×10^3	3×10^3	1×10^3	3×10^2	1×10^2
	$\langle t_w \rangle$	5×10^3	3×10^3	2×10^3	8×10^2	4×10^2	1×10^2

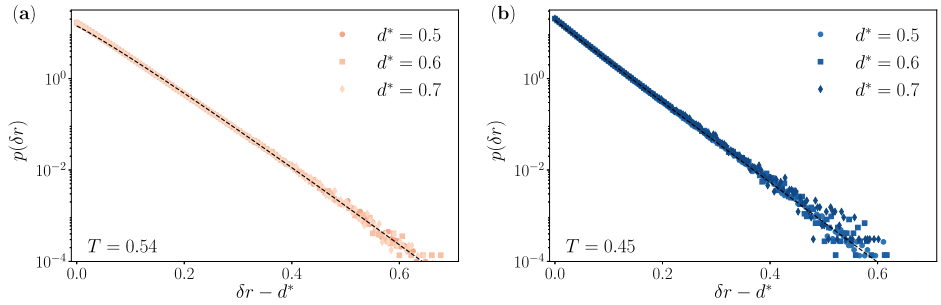

Figure 3. Comparison of jump length distributions for (a) $T = 0.54$ and (b) $T = 0.45$ and varying d^*. The dashed lines represent fits to a compressed exponential function. The obtained values of the compressing exponent do not depend on d^* and are $\alpha = 1.1$ and $\alpha = 1.0$ for panel (a) and (b), respectively.

of the compressing exponent α suggests that at low temperatures (up until $T = 0.5$) the distribution is compatible with a pure exponential function. At higher temperatures (from $T = 0.54$ on) we start observing a deviation from the exponential behaviour indicating the presence of a mixture of exponential and Gaussian behaviour. Indeed, it is expected that by increasing the temperature the Gaussian contribution will become more and more relevant. Concerning the waiting time distribution, the values obtained for β and t_0 grow with lowering temperature, i.e. the higher the temperature the smaller their values. This result suggests that at higher temperature the exponential trend controls the tail of the distribution. On the other hand, at lower temperatures the power law trend becomes more and more pronounced, while the exponential cut off moves to larger and larger waiting times. This observation is in agreement with the fact that at lower temperature the emergence of dynamic heterogeneities makes it more and more

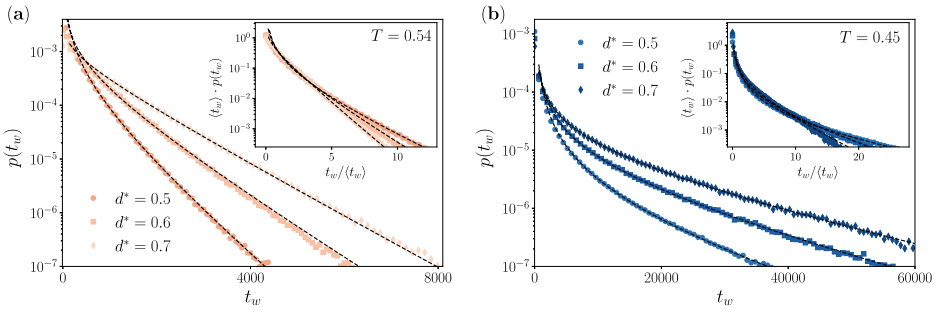

Figure 4. Comparison of waiting time distributions for (a) $T = 0.54$ and (b) $T = 0.45$ and varying d^*. In the insets we report the waiting time distribution properly rescaled over its average value. The dashed lines represent fits to an exponentially truncated power law. The obtained values of the coefficients decrease when increasing d^*. In particular for panel (a) we have $\beta \in [0.3, 1.0]$ and $t_0 \in [1 \times 10^3, 2 \times 10^3]$ while for panel (b) $\beta \in [0.9, 1.5]$ and $t_0 \in [5 \times 10^5, 6 \times 10^5]$.

difficult to identify a single time scale, thus causing the distribution to change from a pure exponential to a truncated power law, with a truncation that happens at a value t_0. Interestingly, if we compare the value of t_0 with the diffusive time t_d discussed in figure 1 we observe that $t_0 \approx t_\mathrm{d}$ (see SM). This observation suggests that by analysing the waiting time distribution we can get an estimate of the diffusive time and thus obtain some insights on the onset of the BnG regime.

In figures 3 and 4 we study the dependence of our results on d^*. Note that we report here plots for two temperature values only, however our results are verified for all the temperature values listed in table 1 (see SM). On the one hand we observe that the jump length distribution remains unchanged when varying d^* (figure 3). On the other hand the waiting time distribution, even if maintaining the same functional behaviour, shows a dependence on d^* which is reflected on the dependence on the coefficients β and t_0 on d^* (see table 1). Note that mostly it is the value of β that is affected while t_0 remains quite stable when changing d^*, ensuring that the analysis discussed above on the BnG regime is not dependent on the value of d^* that we select. The dependence on d^* of the waiting time distribution can be easily understood by focusing on the detection algorithm. For small values of d^* the algorithm is likely to include in the statistics those contributions that actually do not correspond to real jumps but are rather coming from the vibrational motion within the cage. This leads to a slight underestimation of the average waiting time (see table 1) and to two different effects on the distribution: (i) a more prominent peak arises at short waiting times and (ii) the very long waiting times are not detected, and thus the distribution will show a smaller domain of t_w. This is indeed what we observe in figure 4. Moreover, in the insets of figure 4 we report the waiting time distributions normalised over their average values. Regardless of the temperature we observe that the curves for the three values of d^*, when renormalised, collapse into a single one up until at least $5 \cdot \langle t_\mathrm{w} \rangle$, which represents an agreement for a quite large temporal domain.

5. Correlation between waiting times

Figure 5 shows the jumps timeline of particle trajectories in which we display the series of jumps detected along the same trajectory analysed with all the three values of d^*. Once

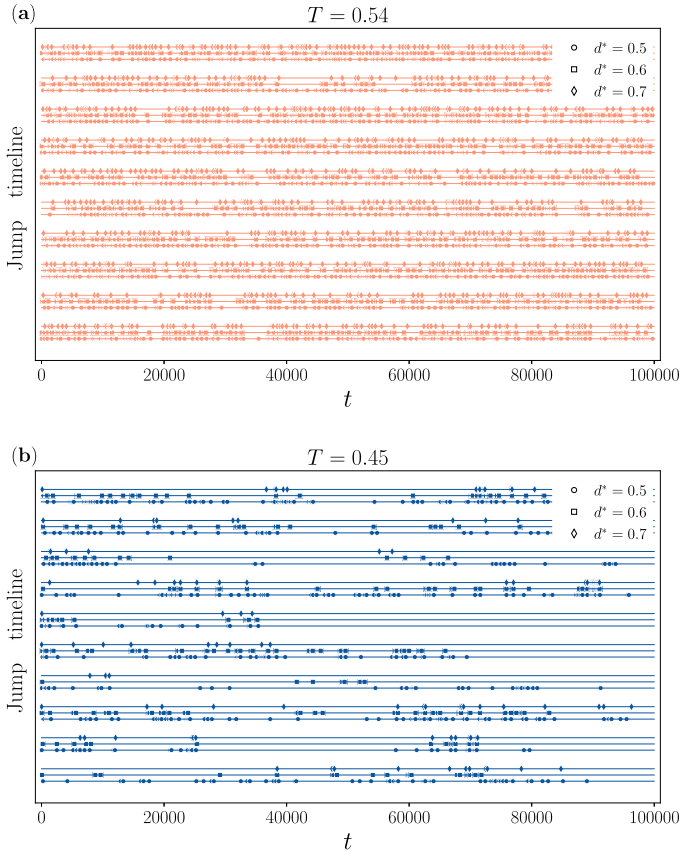

Figure 5. Timelines of ten trajectories analysed with different values of d^* for $T = 0.54$ (panel (a)) and $T = 0.45$ (panel (b)). Each group of three lines represent the same trajectory analysed with the three different value of d^*—as suggested by the legend—and each marker represents a detected jump.

again our discussion here is mostly focused on two temperature values but our results are verified for all the temperature values listed in table 1 (see SM). For the higher temperature ($T = 0.54$) reported in figure 5(a) the jumps seem to be distributed quite equally along the trajectory, regardless of the value of d^*. For the lower temperature ($T = 0.45$) reported in figure 5(b) the picture is quite different. The jumps do not seem to be distributed evenly but they are concentrated within the same time intervals, no matter the value of d^*, showing the fitness of our algorithm to detect jumps. Moreover one can immediately observe that the hopping events group together. For smaller values of d^* this is in part due to the contributions coming from the vibrational motion within the local cage, as described above for the waiting time distribution. However this effect seems to persist also for the biggest value of d^*, suggesting the presence of correlations between waiting times. In particular, we can confirm this observation by selecting a waiting time and study the distribution of its subsequent waiting times. We report this analysis in figure 6. For $T = 0.54$, figure 6(a), all the distributions of subsequent waiting times $p(t_{\rm w}^{n+1})$ collapse together regardless of the selected waiting time $t_{\rm w}^n$, indicating that there is no correlation between waiting times. On the other hand, the plot for $T = 0.45$ reported in figure 6(b) shows that: (i) the smaller the selected

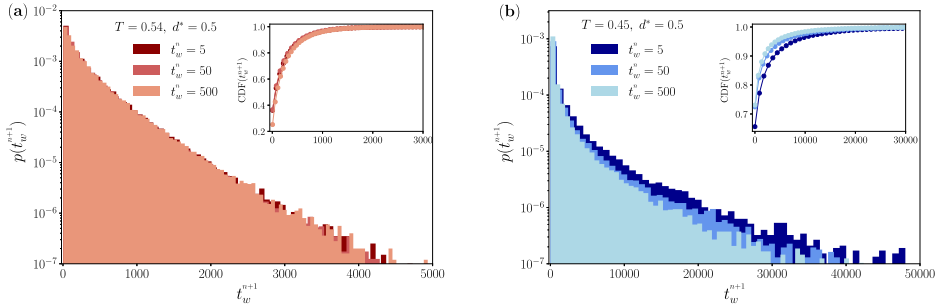

Figure 6. Distributions of subsequent waiting times of selected waiting times $t_{\mathrm{w}}^n = 5, 50, 500$ for $d^* = 0.5$ and (a) $T = 0.54$ and (b) $T = 0.54$. In the inset we show the corresponding cumulative distribution function.

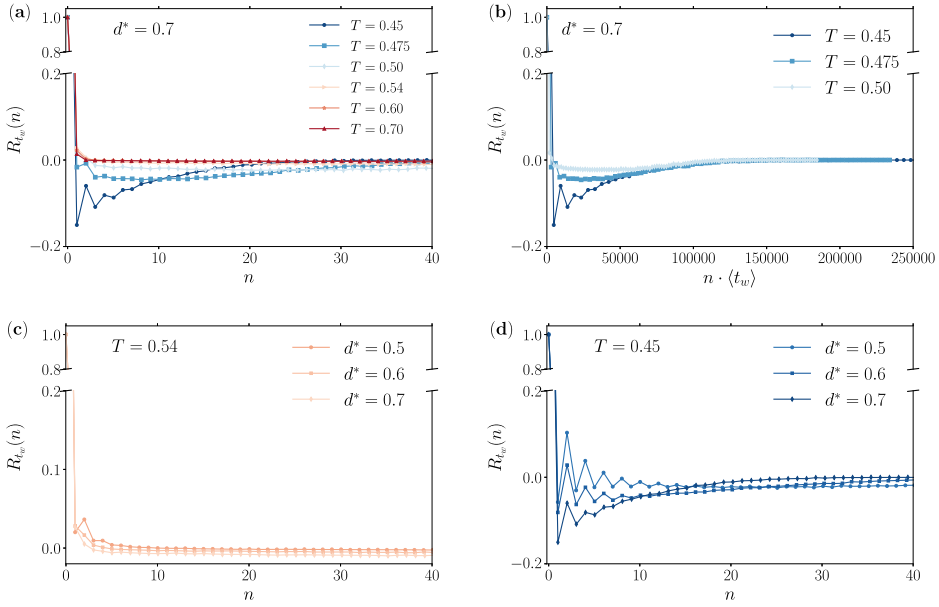

Figure 7. Autocorrelation function of waiting times obtained as defined in (3) for (a) $d^* = 0.7$ and different values of temperature. In panel (b) we report the autocorrelation function for the three lower values of temperature with the x–axis rescaled by the corresponding average waiting time. Panels (c) and (d) show the autocorrelation function for different values of d^* and $T = 0.54$ and $T = 0.45$, respectively.

waiting time t_{w}^n the fatter the tails of the subsequent waiting times distribution $p(t_{\mathrm{w}}^{n+1})$ and (ii) the larger the selected waiting time t_{w}^n the more $p(t_{\mathrm{w}}^{n+1})$ is peaked around short waiting times (see figure 6(b)—inset). We confirmed these observations by performing the 2-sample Kolmogorov–Smirnov test, a nonparametric test that checks whether the two samples have identical distribution [65]. With a level of significance of 1% we observe that for $T = 0.54$ we cannot reject the null hypothesis, that is all datasets share the same distribution. Conversely, for $T = 0.45$, the null hypothesis is rejected and thus the datasets result to come from different distributions (see SM for more details). This analysis confirms the presence of negative

correlations among waiting times at low temperatures. We thus proceed in studying such correlations. Following a standard definition, the autocorrelation function of waiting times can be estimated as [64]

$$R_{t_{\rm w}}(n) = \frac{1}{N_{\rm A}} \sum_{i=0}^{N_{\rm A}} \left(\frac{1}{(N_{\rm J}^i - n)\sigma_{\rm w}^2} \sum_{k=1}^{N_{\rm J}^i - n} \left(t_{\rm w}^k - \mu_{\rm w}\right)\left(t_{\rm w}^{k+n} - \mu_{\rm w}\right) \right), \tag{3}$$

for any positive integer $n < N_{\rm J}^i$, where $N_{\rm J}^i$ is the total number of jumps detected for each particle i and $\mu_{\rm w}$ and $\sigma_{\rm w}^2$ represent the mean and variance of the waiting times, respectively. The sum over i accounts for the average over the ensemble of waiting time series obtained from the $N_{\rm A}$ particles of species A. The curves obtained from our data by implementing equation (3) are reported in figure 7. As expected, our results show negative correlations which appear more pronounced when T decreases. In particular in 7(a) we clearly see that there is no correlation at high temperatures down until $T = 0.54$. At $T = 0.5$ we start to observe a slight negative correlation which gets more and more pronounced when further lowering T. Moreover, we observe in figure 7(a) that upon lowering the temperature the minimum of the autocorrelation not only gets deeper but also moves to the left and is accompanied by a faster relaxation. This effect is due to the fact that the correlation is reported in number of waiting times, and not in real time units. Thus, considering that the average waiting time grows when lowering T, the relaxation appears faster in number of waiting times but it is not if considered in real time units, as can be seen in figure 7(b). It is also interesting to understand the dependence on d^* of our results. At lower values of d^* we observe oscillations in the correlation function. This effect seems to be present at all temperatures—see for instance the result for $d^* = 0.5$ and $T = 0.54$ reported in figure 7(c)—but becomes more and more visible at lower temperatures. Figure 7(d) shows the results for $T = 0.45$ where we observe that at small values of d^* the negative correlations are completely obscured by the oscillations. This effect is reduced for larger value of d^* and, in particular, at $d^* = 0.7$ the negative correlations appear very clean (this is the case also when considering even larger values of d^*—see SM). These oscillations are most likely due to those detected jumps which still correspond to the vibrational motion within a cage and that are present for small values of d^* but disappear when d^* is larger. Thus, performing an analysis on the autocorrelation function of waiting times can also provide good insights on the best value to select for the parameter d^* in order to completely exclude contributions from the vibrational motion within a cage.

6. Conclusions

In this work we made use of a simple yet robust algorithm to detect jumps and waiting times to study the temporal correlation of waiting times in the 3D Kob–Andersen system. Before focusing on the study of the correlations we provided an in-depth statistical characterisation of the jump length and waiting time distributions. As far as the jump length distribution is concerned, we showed that at low temperatures it is well described by an exponential function. When increasing the temperature, its behaviour deviates from a pure exponential, indicating a mixture of exponential and Gaussian regimes. Concerning the waiting time distribution, we observed that it can be well described by an exponentially truncated power law, as mentioned already in other works [44–47]. Moreover, we discussed how the properties of the waiting time distribution can provide insightful information on the onset of the BnG regime in glassy systems.

By studying the jump timelines we observed that the waiting times are correlated. Indeed, by evaluating the autocorrelation of waiting times we showed that, when lowering the temperature of the system, negative correlations emerge. The temporal correlations detected in this work at low temperatures, so as the changes in the statistical properties of the jump length and waiting time distributions, can all be linked to the emergence of dynamic heterogeneities in the system. According to this concept each particle will undergo phases of small and large mobility. The introduction of waiting times and jumps simplifies this picture and classifies the motion into mobile and immobile phases. In this way, each particle along its trajectory will experience alternatively mobile and immobile phases. The emergence of negative correlations among waiting times shows that the hopping between the two phases happens through some rearranging jumps, associated to the short waiting times detected right after a long one. In relation to this, a study appeared very recently [67] in which an analysis of the same system reported in this work is performed, highlighting deviations from CTRW and other theoretical macroscopic predictions at low temperatures. Interestingly, the presence of temporal correlations are listed as a possible reason behind such deviations, thus emphasising the relevance of the results reported here.

From a modelling point of view one could use the mathematical framework defined within the CTRW approach to study how these negative correlations can affect other statistical properties such as the MSD and the displacement distribution. The concept of correlated waiting times was studied in [66] but only for positive correlations. The situation with anti-correlated waiting times, to the best of the authors' knowledge, has never been addressed from a mathematical point of view within the CTRW framework. Thus, this work suggests a clear direction for future analytical studies of CTRW with anti-correlated waiting times.

Finally, we emphasise that the analysis reported in this work can be performed and tested on experimental data obtained from single-particle tracking usually by means of fluorescence microscopy techniques (see for instance [10]).

Acknowledgments

VS is grateful to Prof Christos Likos for helpful discussions. VS acknowledges support of the European Commission through the Marie Skłodowska-Curie COFUND project REWIRE, Grant Agreement No. 847693. SR-V acknowledges support of the European Commission through the Marie Skłodowska-Curie Individual Fellowship No. 840195-ARIADNE. AVC acknowledges support of the Polish National Agency for Academic Exchange (NAWA).

Data availability statement

The data that support the findings of this study are available upon reasonable request from the authors.

ORCID iDs

Vittoria Sposini https://orcid.org/0000-0003-0915-4746
Igor M Sokolov https://orcid.org/0000-0002-4688-9162

References

[1] Wang B, Anthony S M, Bae S C and Granick S 2009 Anomalous yet Brownian *Proc. Natl. Acad. Sci. USA* **106** 15160
[2] Wang B, Kuo J, Bae S C and Granick S 2012 When Brownian diffusion is not Gaussian *Nat. Mater.* **11** 481
[3] Guan J, Wang B and Granick S 2014 Even hard-sphere colloidal suspensions display Fickian yet non-Gaussian diffusion *ACS Nano* **8** 3331
[4] Leptos K C, Guasto J S, Gollub J P, Pesci A I and Goldstein R E 2009 Dynamics of enhanced tracer diffusion in suspensions of swimming eukaryotic microorganisms *Phys. Rev. Lett.* **103** 198103
[5] Xue C, Zheng X, Chen K, Tian Y and Hu G 2016 Probing non-Gaussianity in confined diffusion of nanoparticles *J. Phys. Chem. Lett.* **7** 514
[6] Wang D, Hu R, Skaug M J and Schwartz D K 2015 Temporally anticorrelated motion of nanoparticles at a liquid interface *J. Phys. Chem. Lett.* **6** 54
[7] Hapca S, Crawford J W and Young I M 2009 Anomalous diffusion of heterogeneous populations characterized by normal diffusion at the individual level *J. R. Soc. Interface* **6** 111
[8] Matse M, Chubynsky M V and Bechhoefer J 2017 Test of the diffusing-diffusivity mechanism using near-wall colloidal dynamics *Phys. Rev.* E **96** 042604
[9] Samanta N and Chakrabarti R 2016 Tracer diffusion in a sea of polymers with binding zones: mobile vs. frozen traps *Soft Matter* **12** 8554
[10] Wagner C E, Turner B S, Rubinstein M, McKinley G H and Ribbeck K 2017 A rheological study of the association and dynamics of MUC5AC gels *Biomacromolecules* **18** 3654
[11] Oh Y and Sung B J 2018 Facilitated and non-Gaussian diffusion of cholesterol in liquid ordered phase bilayers depends on the flip-flop and spatial arrangement of cholesterol *J. Phys. Chem. Lett.* **9** 6529–35
[12] Chakraborty I and Roichman Y 2020 Disorder-induced Fickian, yet non-Gaussian diffusion in heterogeneous media *Phys. Rev. Res.* **2** 022020
[13] Beck C 2006 Superstatistical Brownian motion *Prog. Theor. Phys. Suppl.* **162** 29
[14] Miyaguchi T, Akimoto T and Yamamoto E 2016 Langevin equation with fluctuating diffusivity: a two-state model *J. Phys. Rev.* E **94** 012109
[15] Chubynsky M V and Slater G W 2014 Diffusing diffusivities: a model for anomalous, yet Brownian diffusion *Phys. Rev. Lett.* **113** 098302
[16] Chechkin A V, Seno F, Metzler R and Sokolov I 2017 Brownian yet non-Gaussian diffusion: from superstatistics to subordination of diffusing diffusivities *Phys. Rev.* X **7** 021002
[17] Jain R and Sebastian K L 2016 Diffusion in a crowded, rearranging environment *J. Phys. Chem.* B **120** 3988
[18] Tyagi N and Cherayil B J 2017 Non-Gaussian Brownian diffusion in dynamically disordered thermal environments *J. Phys. Chem.* B **121** 7204
[19] Lanoiselée Y and Grebenkov D S 2018 A model of non-Gaussian diffusion in heterogeneous media *J. Phys. A: Math. Theor.* **51** 145602
[20] Sposini V, Chechkin A V, Seno F, Pagnini G and Metzler R 2018 Random diffusivity from stochastic equations: comparison of two models for Brownian yet non-Gaussian diffusion *New J. Phys.* **20** 043044
[21] Barkai E and Burov S 2020 Packets of diffusing particles exhibit universal exponential tails *Phys. Rev. Lett.* **124** 060603
[22] Song S, Park S J, Kim M, Kim J S, Sung B J, Lee S, Kim J-H and Sung J 2019 Transport dynamics of complex fluids *Proc. Natl. Acad. Sci. USA* **116** 12733
[23] Hachiya Y, Uneyama T, Kaneko T and Akimoto T 2019 Unveiling diffusive states from center-of-mass trajectories in glassy dynamics *J. Chem. Phys.* **151** 034502
[24] Baldovin F, Orlandini E and Seno F 2019 Polymerization induces non-Gaussian diffusion *Front. Phys.* **7** 124
[25] Hidalgo-Soria M and Barkai E 2020 Hitchhiker model for Laplace diffusion processes *Phys. Rev.* E **102** 012109
[26] Mora S and Pomeau Y 2018 Brownian diffusion in a dilute field of traps is Fickian but non-Gaussian *Phys. Rev.* E **98** 040101
[27] Li Y, Marchesoni F, Debnath D and Ghosh P K 2019 Non-Gaussian normal diffusion in a fluctuating corrugated channel *Phys. Rev. Res* **1** 033003

[28] Bialas K, Luczka J, Hänggi P and Spiechowicz J K 2020 Colossal Brownian yet non-Gaussian diffusion induced by nonequilibrium noise *Phys. Rev.* E **102** 042121
[29] Luo L and Yi M 2018 Non-Gaussian diffusion in static disordered media *Phys. Rev.* E **97** 042122
[30] Luo L and Yi M 2019 Quenched trap model on the extreme landscape: the rise of subdiffusion and non-Gaussian diffusion *Phys. Rev.* E **100** 042136
[31] Postnikov E B, Chechkin A and Sokolov I M 2020 Brownian yet non-Gaussian diffusion in heterogeneous media: from superstatistics to homogenization *New J. Phys.* **22** 063046
[32] Ślęzak J and Burov S 2021 From diffusion in compartmentalized media to non-Gaussian random walks *Sci. Rep.* **11** 5101
[33] Roldán-Vargas S, Rovigatti L and Sciortino F 2017 Connectivity, dynamics, and structure in a tetrahedral network liquid *Soft Matter* **13** 514
[34] Miotto J M, Pigolotti S, Chechkin A V and Roldán-Vargas S 2021 Length scales in Brownian yet non-Gaussian dynamics *Phys. Rev.* X **11** 031002
[35] Rusciano F, Pastore R and Greco F 2022 Fickian non-Gaussian diffusion in glass-forming liquids *Phys. Rev. Lett.* **128** 168001
[36] Brizioli M, Sentjabrskaja T, Egelhaaf S U, Laurati M, Cerbino R and Giavazzi F 2022 Reciprocal space study of Brownian yet non-Gaussian diffusion of small tracers in a hard-sphere glass *Front. Phys.* **10** 893777
[37] Pastore R, Ciarlo A, Pesce G, Greco F and Sasso A 2021 Rapid Fickian yet non-Gaussian diffusion after subdiffusion *Phys. Rev. Lett.* **126** 158003
[38] Pastore R, Ciarlo A, Pesce G, Sasso A and Greco F 2022 A model-system of Fickian yet non-Gaussian diffusion: light patterns in place of complex matter *Soft Matter* **18** 351–64
[39] Kob W and Andersen H C 1995 Testing mode-coupling theory for a supercooled binary Lennard–Jones mixture I: the van Hove correlation function *Phys. Rev.* E **51** 4626
[40] Chaudhuri P, Berthier L and Kob W 2007 Universal nature of particle displacements close to glass and jamming transitions *Phys. Rev. Lett.* **99** 060604
[41] Kob W, Donati C, Plimpton S J, Poole P H and Glotzer S C 1997 Dynamical heterogeneities in a supercooled Lennard–Jones liquid *Phys. Rev. Lett.* **79** 2827
[42] Kegel W K and van Blaaderen A 2000 Direct observation of dynamical heterogeneities in colloidal hard-sphere suspensions *Science* **287** 290–3
[43] Rubner O and Heuer A 2008 From elementary steps to structural relaxation: a continuous-time random-walk analysis of a supercooled liquid *Phys. Rev.* E **78** 011504
[44] Pastore R, Coniglio A and Pica Ciamarra M 2014 From cage-jump motion to macroscopic diffusion in supercooled liquids *Soft Matter* **10** 5724
[45] Pastore R, Coniglio A and Ciamarra M P 2015 Dynamic phase coexistence in glass-forming liquids *Sci. Rep.* **5** 11770
[46] Pastore R, Coniglio A, de Candia A, Fierro A and Pica Ciamarra M 2016 Cage-jump motion reveals universal dynamics and non-universal structural features in glass forming liquids *J. Stat. Mech.* 054050
[47] De Michele C and Leporini D 2001 Viscous flow and jump dynamics in molecular supercooled liquids. I. Translations *Phys. Rev.* E **63** 036701
[48] Doliwa B and Heuer A 2003 Hopping in a supercooled Lennard–Jones liquid: metabasins, waiting time distribution, and diffusion *Phys. Rev.* E **67** 030501
[49] Heuer A, Doliwa B and Saksaengwijit A 2005 Potential-energy landscape of a supercooled liquid and its resemblance to a collection of traps *Phys. Rev.* E **72** 021503
[50] Ahn J W, Falahee B, Piccolo C D, Vogel M and Bingemann D 2013 Are rare, long waiting times between rearrangement events responsible for the slowdown of the dynamics at the glass transition? *J. Chem. Phys.* **138** 12A527
[51] Heuer A, Kunow M, Vogel M and Banhatti R D 2002 Backward correlations and dynamic heterogeneities: a computer study of ion dynamics *Phys. Rev.* B **66** 224201
[52] Helfferich J, Ziebert F, Frey S, Meyer H, Farago J, Blumen A and Baschnagel J 2014 Continuous-time random-walk approach to supercooled liquids. I. Different definitions of particle jumps and their consequences *Phys. Rev.* E **89** 042603
[53] Pastore R, Pesce G, Sasso A and Ciamarra M P 2017 Many facets of intermittent dynamics in colloidal and molecular glasses *Colloids Surf.* A **532** 87–96
[54] Flenner E and Szamel G 2015 Fundamental differences between glassy dynamics in two and three dimensions *Nat. Commun.* **6** 7392

[55] Illing B, Fritschi S, Kaiser H, Klix C L, Maret G and Keim P 2017 Mermin–Wagner fluctuations in 2D amorphous solids *Proc. Natl. Acad. Sci. USA* **114** 1856
[56] Li Y-W, Mishra C K, Sun Z-Y, Zhao K, Mason T G, Ganapathy R and Pica Ciamarra M 2019 Long-wavelength fluctuations and anomalous dynamics in 2-dimensional liquids *Proc. Natl. Acad. Sci. USA* **116** 22977
[57] Kob W and Andersen H C 1994 Scaling behavior in the β-relaxation regime of a supercooled Lennard–Jones mixture *Phys. Rev. Lett.* **73** 1376
[58] Brüning R, St-Onge D A, Patterson S and Kob W 2009 Glass transitions in one-, two-, three-, and four-dimensional binary Lennard–Jones systems *J. Phys.: Condens. Matter.* **21** 035117
[59] Weber T A and Stillinger F H 1985 Local order and structural transitions in amorphous metal–metalloid alloys *Phys. Rev.* B **31** 1954
[60] Karmakar S and Procaccia I 2012 Finite-size scaling for the glass transition: the role of a static length scale *Phys. Rev.* E **86** 061502
[61] Andersen H C 1980 Molecular dynamics simulations at constant pressure and/or temperature *J. Chem. Phys.* **72** 2384
[62] Coslovich D and Pastore G 2007 Understanding fragility in supercooled Lennard–Jones mixtures. I. Locally preferred structures *J. Chem. Phys.* **127** 124504
[63] Frenkel D and Smit B 2002 *Understanding Molecular Simulation* 2nd edn (Cambridge: Academic)
[64] Box G E, Jenkins G M and Reinsel G C 2008 *Time Series Analysis: Forecasting and Control* 4th edn (New York: Wiley)
[65] Graybill F A, Boes D C and Mood A M 1974 *Introduction to the Theory of Statistics* (New York: McGraw-Hill)
[66] Chechkin A V, Hofman M and Sokolov I M 2009 Continuous-time random walk with correlated waiting times *Phys. Rev.* E **80** 031112
[67] Porpora G, Rusciano F, Pastore R and Greco F 2022 Comparing microscopic and macroscopic dynamics in a paradigmatic model of glass-forming molecular liquid *Int. J. Mol. Sci.* **23** 3556